Decay Kinetics and Quantum Yields of Fluorescence in Photosystem I from *Synechococcus elongatus* with P700 in the Reduced and Oxidized State: Are the Kinetics of Excited State Decay Trap-Limited or Transfer-Limited?

Martin Byrdin,* Ingo Rimke,* Eberhard Schlodder,† Dietmar Stehlik,* and Theo A. Roelofs*
*Institute of Experimental Physics, Freie Universität Berlin, D-14195 Berlin, and †Max-Volmer-Institut für Biophysikalische Chemie und Biochemie, Technische Universität Berlin, D-10623 Berlin, Germany

ABSTRACT Transfer and trapping of excitation energy in photosystem I (PS I) trimers isolated from *Synechococcus elongatus* have been studied by an approach combining fluorescence induction experiments with picosecond time-resolved fluorescence measurements, both at room temperature (RT) and at low temperature (5 K). Special attention was paid to the influence of the oxidation state of the primary electron donor P700. A fluorescence induction effect has been observed, showing a ~12% increase in fluorescence quantum yield upon P700 oxidation at RT, whereas at temperatures below 160 K oxidation of P700 leads to a decrease in fluorescence quantum yield (~50% at 5 K). The fluorescence quantum yield for open PS I (with P700 reduced) at 5 K is increased by ~20-fold and that for closed PS I (with P700 oxidized) is increased by ~10-fold, as compared to RT. Picosecond fluorescence decay kinetics at RT reveal a difference in lifetime of the main decay component: 34 ± 1 ps for open PS I and 37 ± 1 ps for closed PS I. At 5 K the fluorescence yield is mainly associated with long-lived components (lifetimes of 401 ps and 1.5 ns in closed PS I and of 377 ps, 1.3 ns, and 4.1 ns in samples containing ~50% open and 50% closed PS I). The spectra associated with energy transfer and the steady-state emission spectra suggest that the excitation energy is not completely thermally equilibrated over the core-antenna-RC complex before being trapped. Structure-based modeling indicates that the so-called red antenna pigments (A708 and A720, i.e., those with absorption maxima at 708 nm and 720 nm, respectively) play a decisive role in the observed fluorescence kinetics. The A720 are preferentially located at the periphery of the PS I core-antenna-RC complex; the A708 must essentially connect the A720 to the reaction center. The excited-state decay kinetics turn out to be neither purely trap limited nor purely transfer (to the trap) limited, but seem to be rather balanced.

INTRODUCTION

Photosystem I (PS I) of oxygenic photosynthetic organisms is a membrane-bound pigment-protein complex that catalyzes the light-induced transmembrane electron transfer from plastocyanin or cytochrome c_6 to ferredoxin (see Golbeck, 1994; Brettel, 1997, for a review). After light absorption in the antenna, excitation energy is transferred to the primary electron donor called P700, a chlorophyll (Chl) dimer with an absorption maximum at 702 nm. From the lowest excited singlet state of P700 an electron is transferred to the primary electron acceptor A_0, a Chl *a* monomer, with an absorption maximum suggested to be around 690 nm (Mathis et al., 1988; Hastings et al., 1994b; Kumazaki et al., 1994). Stabilization of the charge-separated state is accomplished by transfer of the electron along a chain of further electron acceptors: A_1, a phylloquinone, and three [4Fe-4S] clusters called F_X, F_A, and F_B. The electron is ultimately transferred to soluble ferredoxin. The oxidized P700 is rereduced by soluble plastocyanin or cytochrome c_6.

PS I particles containing ~100 Chl *a* and ~20 carotenoids per P700 have been isolated from the thermophilic cyanobacterium *Synechococcus elongatus* as trimers of identical monomers (Fromme and Witt, 1998), the monomer being the minimum functional unit. In the trimeric form PS I has been crystallized. From x-ray diffraction the structure of the complex at a present resolution of 4 Å is available. It identifies the positions of six Chls, two phylloquinones (Klukas et al., 1999), and three iron-sulfur clusters (Schubert et al., 1997) as cofactors in the reaction center (RC) domain. Two of the six Chls have been assigned to P700 (a dimer at the lumenal side of the complex). Two Chls are positioned similarly to the accessory bacteriochlorophylls in RCs from purple bacteria, and two Chls are equivalent to the bacteriopheophytins and constitute A_0. Surrounding the RC domain, the positions and orientations of the tetrapyrrol planes of 83 core-antenna Chls have been identified in an arrangement described as a hollow, elliptical

Received for publication 21 April 1999 and in final form 17 April 2000.

Address reprint requests to Dr. Theo A. Roelofs, Institute of Experimental Physics, Freie Universität Berlin, Arnimallee 14, D-14195 Berlin, Germany. Tel.: +49-30-838(756)6232; Fax: +49-30-838(756)6081; E-mail: theo.roelofs@physik.fu-berlin.de; or to Dr. Eberhard Schlodder, Max-Volmer-Institut für Biophysikalische Chemie und Biochemie, Technische Universität Berlin, Strasse des 17 Juni 135, D-10623 Berlin, Germany. Tel.: +49-30-31422688; Fax: +49-30-31421122; E-mail: e.schl@struktur.chem.tu-berlin.de.

Dr. Roelofs' present address is SRU OP 2000, Robert-Rössle-Klinik, University Hospital Charité, Humboldt University Berlin, Lindenberger Weg 80, D-13122 Berlin, Germany.

A preliminary account of parts of this work was presented at the XIth International Photosynthesis Congress, August 1998, in Budapest (Byrdin et al., 1998).

0006-3495/00/08/992/16 $2.00

cylinder that narrows slightly toward the lumenal side (Schubert et al., 1997). Each of the core-antenna Chls has at least one neighboring antenna Chl within a (center-to-center) distance of 16 Å, whereas for the distance between any core-antenna Chl, except two, and the RC Chls, 16 Å constitutes a minimum value. Only two core-antenna Chls, referred to as linker or connecting Chls, are positioned at a distance of 13 Å and 15 Å from A_0 and provide the closest contact between the core-antenna and RC. For two adjacent monomers within the trimer the shortest Chl-Chl distance is 24 Å.

The excited-state dynamics of various PS I complexes, prepared from several different organisms, have been studied with time-resolved absorption and fluorescence techniques by various groups and with varying time resolution. The preparations used differ inter alia in the degree of spectral heterogeneity of the core-antenna system, i.e., in the content of Chl with absorption maxima greater than 700 nm, the so-called red pigments. Correlation of the number and spectral properties of red pigments with the observed excited-state kinetics is expected to contain information on their functional role. In the case of cyanobacteria at room temperature, PS I core-antenna-RC-complexes from *Synechococcus elongatus* (~9 red Chls: 5 A708 and 4 A720–735; Flemming 1996) exhibit dominant lifetime components of 2–3 ps (Gobets et al., 1998a), 7–12 ps, and 33–37 ps (Holzwarth et al., 1993; Turconi et al., 1993; Gobets et al., 1998a; or resolved into 20 ps and 50 ps, Dorra et al., 1998). In *Synechocystis sp*. (~2 red Chls: 2 A708; Gobets et al., 1994) somewhat shorter lifetimes are found: 0.43 ps, 2–6 ps (recently resolved into two components of 2 ps and 6.5 ps, Savikhin et al., 1999), and 22–28 ps (Hastings et al., 1994a,b, 1995; DiMagno et al., 1995; Savikhin et al., 1999). For *Spirulina* (~6–7 red Chls with in part extremely red-shifted absorption maxima: two A705, one or two A714, one A726, one A737, and one A746; Karapetyan et al., 1997) major lifetime components of 9 ps, 30 ps, and 66 ps were found (Karapetyan et al., 1997). In contrast to the situation in cyanobacteria, PS I core antenna-RC complexes from green algae and higher plants contain fewer red Chls with substantially smaller red shifts.

Based on these experimental data, various models for the excited-state kinetics of PS I have been proposed (e.g., Pearlstein, 1982; Owens et al., 1987; Jia et al., 1992; Holzwarth et al., 1993; Trinkunas and Holzwarth, 1994, 1996, 1997; Laible et al., 1994; Valkunas et al., 1995; White et al., 1996; Jennings et al., 1997; Gobets et al., 1998a; Dorra et al., 1998, Beddard, 1998). Kinetic limitations have been proposed that range from "nearly diffusion-limited" (Owens et al., 1987; Croce et al., 1996) to "essentially trap-limited" (Holzwarth et al., 1993; Dorra, 1998) (see Van Grondelle et al., 1994, for a review).

The fluorescence kinetics and yield are expected to change significantly if photochemistry and, consequently, the main excited-state decay pathway are blocked. In PS I photochemistry can easily be blocked by oxidation of the primary donor P700. This can be achieved either by chemical titration or by illumination in the absence of external electron donors. Throughout this work, the terminus "open PS I" will serve as a synonym for "PS I with P700 in the reduced (noncharged) state," and, on the other hand, "closed PS I" means "PS I with P700 in the oxidized state $P700^+$." (This is different for PS II, where the closed state represents the situation reduced primary donor P680 and reduced acceptor Q_A^-. Thus the primary radical pair $\{P680^+ \ Pheo^-\}$ can still be formed, but stabilization of the charge separation is not possible.) So far, time-resolved measurements of the excited-state decay have not been able to resolve a difference in the kinetics between open and closed PS I (Holzwarth et al., 1993; Turconi et al., 1993; Dorra et al., 1998). Another highly sensitive approach is the so-called fluorescence induction technique, in which light-induced changes in the fluorescence quantum yield are monitored on the time scale of trap closure. In PS II a more than threefold increase in fluorescence yield is observed upon trap closure (for a review see Krause and Weis, 1991). On the other hand, for PS I, only small (if any) fluorescence changes of either positive or negative sign have been reported (Ikegami, 1976; Telfer et al., 1978; Trissl, 1997). On this basis, the oxidized donor $P700^+$ is widely considered to be as good a quencher as the reduced donor P700, although the reason for this is unclear at present.

In this work we combine fluorescence induction experiments with picosecond time-resolved fluorescence measurements in the open and closed RC states of PS I. This opens the important possibility of comparing the dynamics of excitation transfer and decay in two well-defined redox states of P700 in the same sample. These dynamics crucially depend on the mutual assignment of the various spectral forms to the spatial positions of the chlorophylls as resolved by x-ray diffraction, using crystals prepared from the same samples as used in this study. Unfortunately, structural information obtained by x-ray crystallography (even at improved resolution) does not allow for spectral assignment of the individual core-antenna Chls. With respect to the red pigments, further insight is obtained from fluorescence lifetime measurements at low temperature, where quenching occurs via direct transfer from the pigments with redmost absorption maximum to the oxidized primary donor $P700^+$. Their minimum distance from P700 can be estimated by Förster theory, taking into account the spectral overlap with the $P700^+$ absorption spectrum.

The information thus obtained, along with all of the available spectral and structural data, can be used in simulations of energy transfer and trapping with the aim of reproducing the measured excited-state dynamics. Such simulation yields information on the following issues: 1) The decisive role of the red pigments (see Trissl, 1993 for a review). 2) The presence of a rate-limiting step in the excited-state decay dynamics and, if present, its exact na-

ture. This is crucial for extraction of the underlying molecular rate constants, particularly the intrinsic charge separation rate. 3) The different quenching mechanisms in open and closed PS I. Our results suggest that the excited-state decay kinetics is neither purely trap limited nor purely transfer (to the trap) limited, but seems to be rather balanced.

MATERIALS AND METHODS

Sample preparation

Trimeric PS I complexes with ~100 Chl per P700 were isolated from the thermophilic cyanobacterium *Synechococcus elongatus* as described elsewhere (Fromme and Witt, 1998). The material was stored in the dark at −30°C and thawed just before the measurements. For fluorescence induction measurements the sample was resuspended in a buffer containing 20 mM tricine (*N*-[2-hydroxy-1,1-bis(hydroxymethyl)ethyl]glycine, pH 7.5), 20 mM $MgCl_2$, 5 mM sodium ascorbate, and 0.02% *n*-dodecyl-β-D-maltoside (β-DM) to a final Chl concentration of 5 μM. For picosecond fluorescence experiments, samples contained 0.002% β-DM and 8 μM Chl. At room temperature, without further additions, the RCs in these samples remain in the closed state, even under low-light conditions. This was checked by flash-induced absorbance difference spectroscopy. To obtain samples with open RCs, 5 mM sodium ascorbate and 150 μM PMS (phenazine methosulfate) were added. Under these conditions, it was determined that $P700^+$ is reduced with a time constant of ~2 ms. For measurements at cryogenic temperatures, glycerol was added to the samples to a final concentration of 65% (w/v). Samples with closed RCs were prepared by freezing under illumination; samples with initially open RCs were prepared by freezing in the dark in the presence of 5 mM ascorbate. Both fluorescence induction and picosecond fluorescence kinetics were measured upon laser excitation around 630 mm. into the weakly structured absorption band of the Chl pigments around 630 mm. This ensures that all Chls are excited with (almost) equal probability, independently of the exact localization of their individual $Q_{Y(0-0)}$ absorption maximum.

Fluorescence induction

Fluorescence was excited with a He-Ne laser at 633 mm. An electrically controlled mechanical shutter with a 10–90% rise time of ~1 ms allowed us to expose the sample to the excitation beam for a chosen time period. The fluorescence of the sample contained in a 10 mm × 10 mm cuvette was excited near the edge of the cuvette (avoiding self-absorption) and recorded at a right angle to the excitation beam by a photomultiplier (EMI 9668-BQ) shielded by a long-pass filter with a cutoff wavelength of 665 nm and connected to a transient recorder (Tektronix TDS 540), which was triggered by the shutter driving electronics. The dependence of the fluorescence induction effect on the redox potential of the sample was determined by redox titration as described previously (Webber et al., 1996). For measurements at cryogenic temperature the cuvette was placed in a liquid nitrogen bath cryostat (Oxford DN1704) or in a continuous-flow helium cryostat (Oxford CF1204), either frozen in the dark in the presence of 5 mM ascorbate (open RCs) or frozen under illumination (closed RCs).

Picosecond fluorescence measurements

Picosecond fluorescence measurements were made by time-correlated single-photon counting (TCSPC), using 10-ps (full width at half-maximum, FWHM), 631-nm excitation pulses at a 4-MHz repetition rate from a cavity-dumped DCM dye laser (375/344 Spectra Physics) synchronously pumped by a mode-locked Ar ion laser (2045-15; Spectra Physics). Fluorescence was subsequently selected by a polarizer set at the magic angle with respect to the polarization of the excitation beam and a double monochromator (Jobin Yvon DH10-VIS) with a spectral bandwidth of 5 nm FWHM, and detected by a microchannel plate photomultiplier (Hamamatsu R3809U-01 with an extended multialkali photocathode). This yields a temporal instrument response function of, typically, ~40 ps FWHM. The excitation intensity was sufficiently low to ensure fewer than 0.0005 photons absorbed per PS I per pulse (i.e., 2000 excitations/PS I/s). Thus annihilation effects can be excluded. At room temperature (RT) the sample was pumped through a 2 mm × 2 mm flow cuvette (Starna) at a rate of 36 ml/min; the detection geometry was rectangular. For measurements on open samples, the intensity of the excitation beam had to be reduced further by a factor of 40, resulting in 50 excitations/PS I/s; thus ~90% of the centers were found in the open state. To maintain a sufficient count rate under such low-light conditions, the spectral bandwidth for detection was extended to 10 nm and the spatial aperture for detection was enlarged, resulting in a broadening of the instrument response function.

For low-temperature measurements the beam geometry was changed to backface excitation (i.e., almost 180°) to minimize artifacts due to scattered light. In this case a 0.1-mm cuvette (Starna) was used, and the Chl concentration was increased to 160 μM, resulting in the same optical density as for RT measurements. The cuvette was placed in a continuous-flow helium cryostat (Oxford CF 1204) at 5 K.

Data analysis

Fluorescence decays (5 ps per channel, >30,000 counts in the peak channel) detected at different wavelengths were deconvoluted with the measured instrument response function and simultaneously fitted to a sum of exponentials with a common set of lifetimes (global analysis), minimizing the sum of weighted squared residuals, using the Globals Unlimited software Package developed at the Laboratory for Fluorescence Dynamics at the University of Illinois (Beechem et al., 1991). The resulting amplitudes for each decay component were normalized in such a way that their yields (i.e., amplitude multiplied by lifetime) sum up to the in situ detection-system-corrected steady-state emission spectrum of the sample. The longest lifetime was determined by a fit over a 5-ns range of the data; subsequently this lifetime was kept fixed during a fit over a shorter data range of 1.5 ns, with all other (shorter) lifetimes free running. The error intervals for the lifetimes were determined by an "exhaustive search" analysis (Beechem et al., 1991) and correspond to a confidence level of 67%.

Kinetic modeling

Kinetic modeling was based on Förster theory (for a discussion on its applicability see, e.g., Borisov, 1989; for its extension to the intermediate coupling case, see Kakitani et al., 1999) in a way similar to that described by Gobets et al. (1998a,b). The Förster theory makes it possible to calculate the rate of energy transfer k_{ij} between two pigments as follows:

$$k_{ij} = C \cdot \frac{\kappa^2 \cdot \mathrm{FOI}}{n^4 \cdot \tau_0 \cdot R_{ij}^6} = \frac{1}{\tau_0} \cdot \left(\frac{R_0}{R_{ij}}\right)^6,$$

where R_{ij} is the distance between the pigments, κ describes the mutual orientation of the transition dipol moments, n is the refractive index of the local environment, FOI is the spectral overlap between the donor's emission spectrum and the acceptor's absorption spectrum, τ_0 is the natural fluorescence lifetime, and C is a constant. The so-called Förster radius R_0 is defined as the distance for which the probabilities for resonance energy transfer and fluorescence are equal. For spectrally identical chlorophyll *a* molecules R_0 is found to be 6.5–8.5 nm (Colbow, 1973; Van Grondelle, 1985).

The distances between the central Mg atoms of the chlorophylls were taken from the coordinates of the 89 Chls resolved so far by x-ray

diffraction and deposited in the Brookhaven Protein Databank as 2pps.bpd (Schubert et al., 1997). The influence of the orientation of the transition dipoles could not be considered explicitly. Thus far, the relative dipol orientation is known only with respect to the angle between each pair of Chl planes but not with respect to the orientation in the plane. The orientational information can be readily inserted as it becomes available. At present just an averaged orientational value of $\kappa^2 = 0.67$ is considered. Decomposition of the 5 K absorption spectrum (see below) yielded seven distinct spectral forms with Q_Y absorption maxima between 668 nm and 720 nm. For the sake of simplicity, P700 was accounted for by additional introduction of two equivalent Chls with absorption maxima at 702 nm, neglecting excitonic interaction. Overlap integrals were calculated using the Chl spectra of Shipman and Housman (1979), as modified by Laible (1995), with a uniform Stokes shift of 130 cm^{-1} for all pigments, to fulfill the detailed balance condition. After assignment of the spectral forms to the spatial positions, a matrix of 89 $\times$ 89 transfer rates k_{ij} is calculated according to the Förster equation, with $n = 1.45$ and $\tau_0 = 15$ ns (Colbow, 1973). The introduction of a common scaling factor for the rate constants reflects uncertainties in the knowledge of n, τ_0, and the exact spectral shape of a single Chl in a protein environment. The transfer matrix T is calculated from the 89 $\times$ 89 rate matrix by replacement of the elements on the main diagonal with the respective depopulation rates. Fluorescence lifetimes were obtained as the reciprocal eigenvalues of T, determined numerically. The associated amplitudes result from the respective eigenvectors after weighting with the initial excitation distribution. Here stoichiometric excitation was used, i.e., each of the 89 Chls per complex is excited with equal probability. The amplitudes for all pigments of each spectral pool were summed up and plotted against absorption wavelength as simulated decay-associated spectra (SDAS). These SDAS reflect population changes of the various spectral pools occurring with various lifetimes. After Stokes-shifting and Gauss-enveloping the SDAS can be compared to the measured fluorescence DAS. In addition to the assignment of the spectral forms to the spatial positions, only two parameters can be varied to optimize the agreement between simulated and observed spectra and lifetimes: the intrinsic charge separation rate constant from P700 and the scaling factor of the rate matrix with respect to the time scale (physically equivalent to a variation of the Förster radius). More details on the simulation can be found elsewhere (Byrdin, 1999).

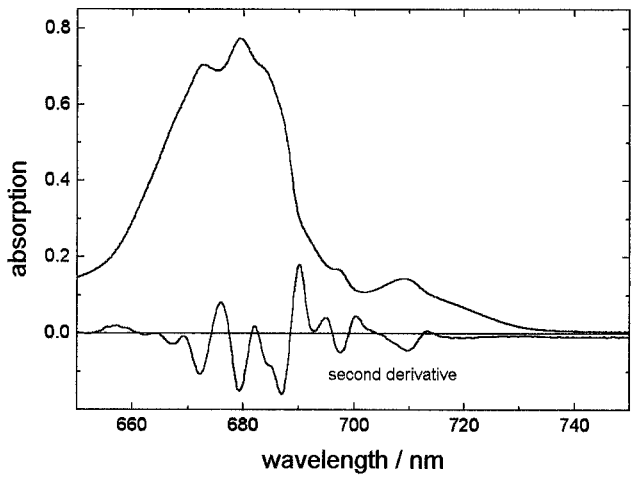

FIGURE 1 5 K absorption spectrum and its second derivative of the PS I core-antenna-RC complex from *Synechococcus elongatus* used throughout this work. Note that the absorption extends beyond 740 nm.

RESULTS

Decomposition of the PS I low-temperature absorption spectrum

The absorption spectrum in the Q_Y region of the trimeric PS I complexes from *Synechococcus elongatus* at 5 K, as shown in Fig. 1, exhibits a pronounced structure due to the spectral heterogeneity of the Chl chromophores. The minima in the second derivative of this spectrum (see Fig. 1) are taken as an indication of the wavelengths of maximal absorption of the various pigment pools. A satisfactory Gaussian decomposition of the spectrum is achieved by using at least seven different pools of pigments. To allow for different degrees of inhomogeneous broadening of the pools, the width of the Gaussian bands was allowed to vary for the different pools. In addition, an eighth band was introduced at 702 nm to explicitly account for P700 constituted by two chlorophylls. The relative areas under the Gaussian curves yield the following decomposition of the PS I core antenna-RC complex (Flemming, 1996): 40 Chls absorbing maximally around 668 nm, 12 Chls at 674 nm, 8 Chls at 679 nm, 23 Chls at 685 nm, 6 Chls at 695 nm (A695), 2 Chls at 702 nm attributed to P700, 5 Chls at 708 nm (A708), and 4 Chls at 720 nm (A720). We are fully aware of the limitations of such decompositions, but in the red part of the spectrum (>700 nm) in particular it yields a reliable estimate of the amount of red pigment involved, which turns out to play a crucial role in the excitation dynamics. The lower amount of A720 (only one pigment at 720 nm) reported earlier (e.g., Trinkunas and Holzwarth, 1994) is probably due to the use of Triton X-100 during the preparation of the PS I complexes, resulting in the loss of some of the long-wavelength pigments. The PS I complexes used in this study contain nine so-called red pigments, i.e., Chls with an absorption maximum at wavelengths longer than that of P700. The existence of these red pigments argues for the good quality of the PS I preparation. For the redmost pool A720, an exceptionally broad spectral width of 18 nm (FWHM, as compared to an average of 10 nm FWHM for the other pools) was used to account for the wide tail of the absorption spectrum at the red side indicating a broad distribution of the absorption maxima of the redmost pigments between 720 nm and 740 nm. This is supported by the finding of pigment(s) with an emission maximum as far out as 747 nm (see below) and by the dependence of the emission maximum on the excitation wavelength for $\lambda_{exc} >$ 725 nm (Pålsson et al., 1996).

Fluorescence induction at room temperature

As mentioned, fluorescence induction experiments monitor the change in fluorescence quantum yield upon illumination which leads to closure of the RC, i.e., in the case of PS I, due to light-induced oxidation of P700. Fig. 2 shows the time course of the fluorescence intensity detected after the

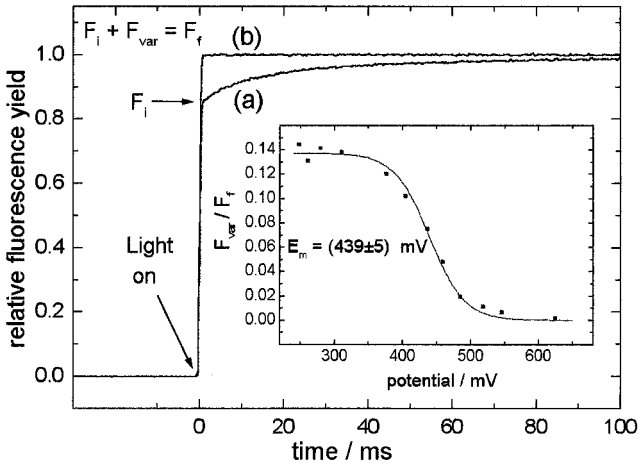

FIGURE 2 Changes in the fluorescence yield upon illumination (fluorescence induction curves) of (*a*) open PS I (P700 initially reduced) and (*b*) closed PS I (P700 oxidized) at room temperature. *Inset*: Redox titration of the normalized variable fluorescence, i.e., $F_{var}/F_f = (F_f - F_i)/F_f$.

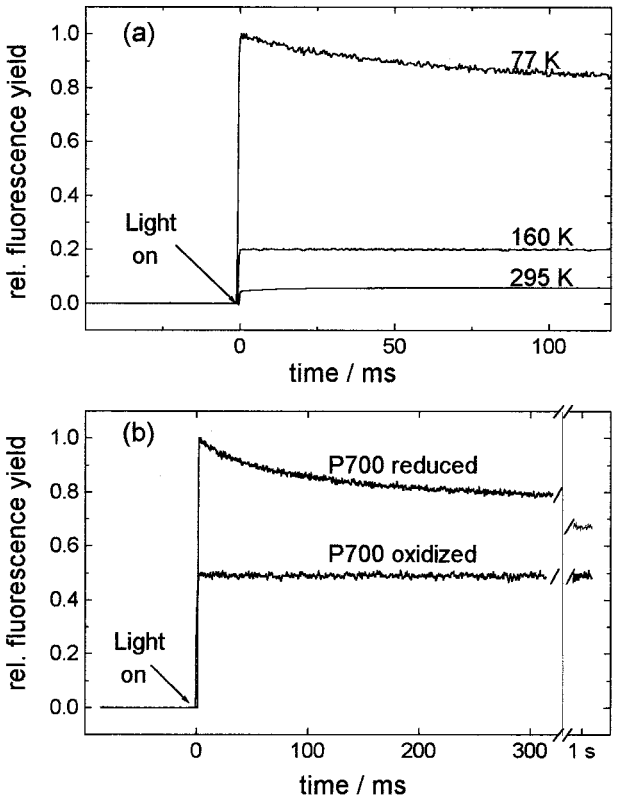

FIGURE 3 (*a*) Changes in the fluorescence yield upon illumination (fluorescence induction curves) of open PS I at various temperatures. (*b*) Fluorescence induction curves at 5 K. *Top trace*: initially open PS I. *Bottom trace:* closed PS I. Note that for initially open PS I, the final fluorescence level, F_f, is not reached before ~1 s of illumination. This final level is attributed to a mixture of ~50%/~50% of open/closed PS I (see text for details).

excitation light is switched on (at time 0). Trace a was obtained for a sample with initially open RCs prepared by dark incubation in the presence of ascorbate. The fluorescence yield clearly rises from an initial value F_i to a final value F_f. The total amplitude change, the so-called variable fluorescence $F_{var} = F_f - F_i$, amounts to ~(12 ± 5)% of the final value F_f, varying somewhat with sample preparation. Trace b was obtained when the sample was preilluminated, i.e., with closed RCs. No change in fluorescence yield could be detected in this case, suggesting that the increase in fluorescence yield upon illumination is indeed due to the photooxidation of the primary donor P700. To further substantiate this, a redox titration of the normalized variable fluorescence was performed (Fig. 2, *inset*). A Nernst fit (*solid line*) to the titration curve (*squares*) reveals a midpoint potential of 439 ± 5 mV. This value is in good agreement with the reported midpoint potential of 436 ± 5 mV for the oxidation of P700 in identical PS I core-antenna-RC preparations from *S. elongatus*, as determined by the amplitude of absorbance change attributed to flash-induced oxidation of P700 as function of the potential (Webber et al., 1996).

Fluorescence induction at low temperature

To investigate thermal equilibration of the excitation energy among the various spectral pigment pools, we made fluorescence induction measurements at various temperatures down to 5 K. Fig. 3 *a* shows time traces at 295 K, 160 K, and 77 K for samples with initially open RCs. There are two obvious effects: first, the initial and final fluorescence yields increase with decreasing temperature; second, the induction effect vanishes around $T = 160$ K and reappears at lower temperatures but with opposite sign. The latter indicates that the fluorescence quenching efficiency of $P700^+$ relative to that of P700 increases with decreasing temperature. Fig. 3 *b* shows the fluorescence induction transients at 5 K, for a sample with initially open RCs (*top trace*) and for a sample with initially closed RCs (*bottom trace*). Comparison of Fig. 3 *b* with Figs. 2 and 3 *a* reveals, first, that the time needed to reach the final fluorescence level F_f increases with decreasing temperature, and second, that at low temperatures even prolonged illumination does not lead to the fluorescence level displayed by samples with initially closed RC. These effects indicate that below a certain temperature dark-frozen samples with open RCs cannot be completely closed by illumination. This observation agrees well with recent findings that below a certain temperature forward electron transfer from A_1^- to F_X is frozen out in a fraction of PS I (~50% at 5 K), leading to charge recombination of $\{P700^+ A_1^-\}$ at a rate of $\sim 4 \times 10^3\ s^{-1}$ (Schlodder et al., 1998). The excitation rate of the actinic light is at least one order of magnitude below this value; thus PS I is kept in the open state in this fraction.

Fig. 4 shows the temperature dependence of the relative fluorescence yield for samples with completely open RCs (*triangles*) and closed RCs (*squares*). These values were derived from the initial value of the fluorescence induction traces (Figs. 2 and 3). In addition, the final fluorescence level reached by illumination of samples with initially open RCs at 5 K is shown (*circle*). From room temperature down to 5 K, the fluorescence yield increases by a factor of ~20 for open PS I, as compared to a factor of ~10 for closed PS I.

To obtain further information on the underlying mechanisms for the dependence of the fluorescence quantum yield on temperature and on the redox state of P700, we performed picosecond time-resolved fluorescence experiments, at both RT and 5 K, on samples with open and closed RCs.

Picosecond fluorescence kinetics at room temperature

Time-correlated single photon counting measurements on the picosecond time scale were performed on PS I samples with the RCs in both open and closed states at RT. The in situ recorded (i.e., with the single photon timing apparatus under the conditions used for the decay measurements), detector-corrected steady-state fluorescence spectra for samples with open and closed RCs are compared in Fig. 5. The area enclosed by the spectrum for open PS I is smaller than that for closed PS I by ~8%. This agrees well with the findings of the fluorescence induction experiments (see above). Within the resolution of the data, no significant difference in spectral shape between 680 nm and 790 nm could be detected for open versus closed PS I.

Fluorescence decays (see examples in Fig. 7), detected for a set of closely spaced wavelengths in the spectral range from 665 nm to 745 nm, were analyzed globally. Fig. 6 shows the resulting DAS for closed RCs, which will be discussed first. The set of four lifetime components needed to fit the decays is 13 ± 2 ps, 37 ± 1 ps, 170 ± 40 ps, and 2.1 ± 0.2 ns. The shortest resolved lifetime component, 13 ± 2 ps, is associated with a spectrum that exhibits both positive amplitudes at wavelengths less than 700 nm and negative amplitudes at wavelengths greater than 700 nm. Such a DAS is related to excitation energy transfer from Chls absorbing below 700 nm to the red pigments, reflected by a fluorescence decay below 700 nm and a corresponding fluorescence rise term for wavelengths greater than 700 nm

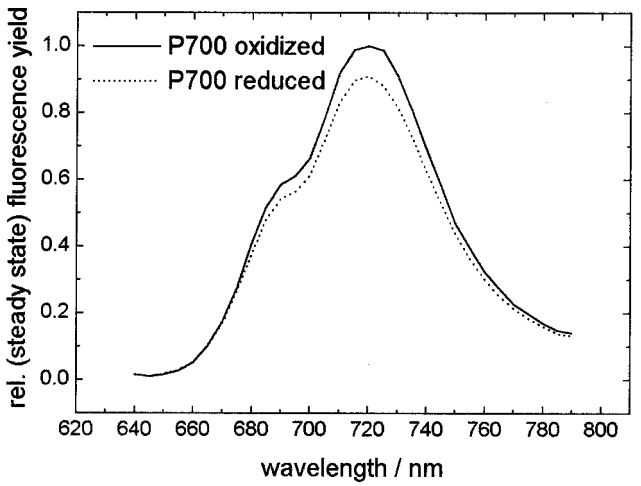

FIGURE 5 In situ recorded, detector-corrected steady-state fluorescence yield spectra of the PS I complexes with P700 reduced (– – –) and P700 oxidized (——). The spectra are normalized to the maximum fluorescence yield obtained for closed PS I.

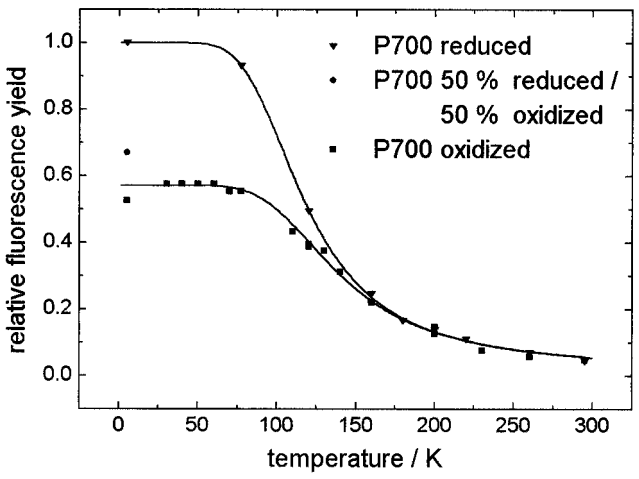

FIGURE 4 Temperature dependence of the relative fluorescence yield for samples with P700 reduced (open PS I, ▽), with P700 oxidized (closed PS I, ■), and with a mixture of ~50%/~50% of P700 reduced/oxidized (●).

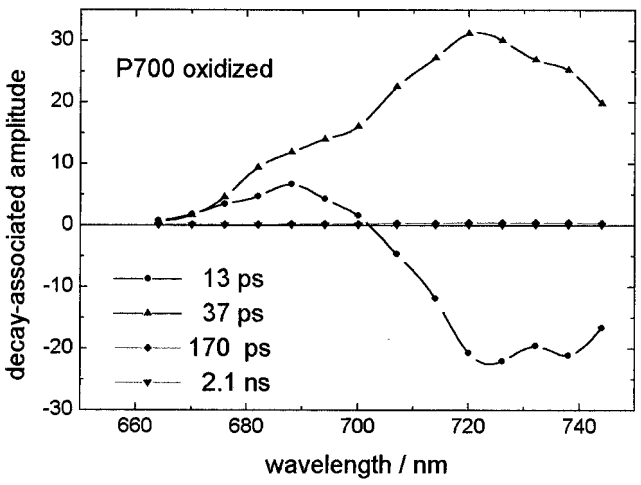

FIGURE 6 Decay-associated fluorescence spectra (DAS) for PS I samples with P700 oxidized (closed PS I) at room temperature. The two longer components (170 ps and 2.1 ns) have a very small amplitude. Note the nonconservative transfer spectrum associated with the 13-ps lifetime.

(Holzwarth et al., 1993; Turconi et al., 1993; Hastings et al., 1994a; Dorra et al., 1998; Gobets et al., 1998a). Remarkably, the areas enclosed by the horizontal axis and the positive part of the spectrum (<700 nm) on one hand and the negative part on the other hand are clearly not equal. If the DAS reflected only energy transfer, a conservative spectrum would be expected. Possible origins for nonconservative DAS are discussed below. The lifetime of the dominant decay component (~95% of the decay amplitude in its maximum) is 37 ps, which can be determined to an accuracy of ±1 ps. This component exhibits an all-positive amplitude peaking around 720 nm, with a shoulder around 690 nm. This component is ascribed to the overall decay of the excited states, in accordance with the literature (Werst et al., 1992; Holzwarth et al., 1993; Turconi et al., 1993, 1994; Hastings et al., 1994a; Pålsson et al., 1995; Dorra et al., 1998; Gobets et al., 1998a). Two additional components of minor amplitude (<5%; see Fig. 6) and less well defined lifetimes were found. The peak of the longest component, 2.1 ± 0.2 ns, is clearly blue-shifted (not visible in Fig. 6) and is therefore attributed to a small amount of uncoupled Chls (i.e., Chls not involved in the transfer of excitation energy to the RC). The other component, 170 ± 40 ps, peaks around 730 nm; its origin is unclear at present.

It should be noted that the error intervals indicated above do not account for biochemical sample-to-sample variation, which can be on the order of 10%. To allow the identification of changes in lifetimes and/or relative amplitudes on the order of 10%, it is necessary to perform the measurements of the open and closed RC states on one and the same sample. To maintain the open RC state it is absolutely essential to measure the fluorescence decay kinetics at very low excitation intensity, even in the presence of an artificial electron donor. To maintain a sufficiently high count rate, it was necessary to reduce the temporal and spectral resolution (see Materials and Methods). The quality of the fit is correspondingly lower. Nevertheless, as for closed centers, a similar set of four lifetimes could be resolved. Although the transfer component could not be resolved well, the lifetime of the dominant decay component has been determined with high precision to 34 ± 1 ps. The corresponding DAS closely resembles the one observed for the 37-ps component in closed PS I (see Fig. 6). The difference in the lifetimes of the main decay components in open and closed PS I is clearly visible from the unprocessed (convoluted) decay curves as presented in Fig. 7. One was obtained immediately after the other on the same sample. First, the sample was excited with very low intensity, but in the absence of any artificial electron donor. Thus the RC was in the closed state despite the low excitation intensity. Subsequently, ascorbate and PMS were added, and the RCs remained open in ~90% of the PS I complexes under the same excitation conditions. Obviously, this approach reveals a significant difference in the width of the time curves for open RCs (*dashed line*) and closed RCs (*solid line*) of 3.6 ps FWHM.

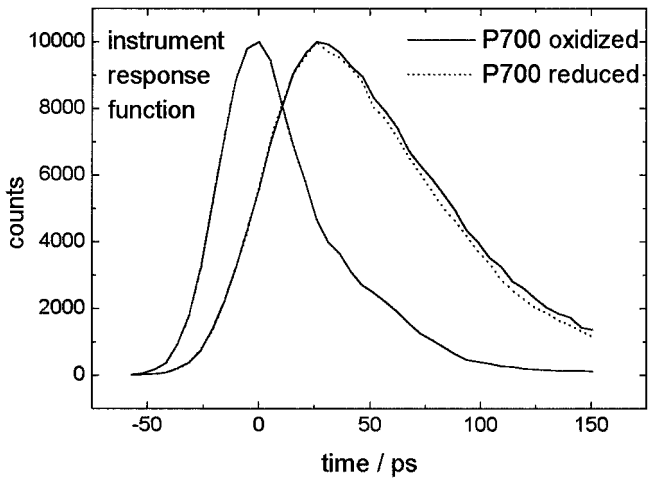

FIGURE 7 Fluorescence decay curves for PS I samples with P700 oxidized (closed PS I, ——) and P700 reduced (open PS I, – – –) for excitation at 631 nm and detection at 707 nm. Note that these raw decay data represent a convolution of the decay kinetics with the normalized instrument response function (shown at the *left side*, peaking at zero time).

To exclude the occurrence of nonspecific quenching by the added chemicals, a cross-check was performed. The excitation intensity was increased subsequently to a level sufficient to keep P700 photooxidized, even in the presence of ascorbate and PMS. (Simultaneously the aperture for detection had to be reduced to limit the detection count rate, thus changing the width of the instrument response function (40 ps instead of 43 ps). This makes a direct comparison with the raw (convoluted) data presented in Fig. 7 difficult.) Indeed, the lifetime of the main decay component was determined to 37 ps once again, i.e., the value expected for closed PS I (not shown). Thus the difference in fluorescence yield as found in the RT fluorescence induction experiment (Fig. 2) and confirmed by the RT steady-state fluorescence spectra (Fig. 5) is found to be due mainly to an increase in the overall excited-state decay lifetime for closed RCs (37 ps) as compared to open RCs (34 ps). In open RCs this decay occurs via charge separation, whereas in closed RCs a different quenching mechanism has to be responsible (see below). Lifetimes and DAS of the intermediate (210 ± 40 ps) and long-lived (2.1 ± 0.2 ns) components do not differ significantly from those of closed centers.

Picosecond fluorescence kinetics at 5 K

Low-temperature fluorescence decay kinetics were determined for samples with all RCs in the closed state and for samples containing a mixture of open and closed RCs. Samples with all RCs closed were prepared by freezing the sample under illumination. On the other hand, freezing a sample containing ascorbate (which keeps both P700 and the acceptors in the neutral state) under complete darkness leads to a sample with all RCs initially in the open state.

Low-temperature illumination of such a sample will lead to the irreversible formation of the radical pair $\{P700^+ F_{A/B}^-\}$ in a fraction (~50% at 5 K) of the RCs, whereas in the other RCs a charge recombination of $\{P700^+ A_1^-\}$ maintains the open RC state (see above). Thus it is possible to prepare samples containing a substantial fraction (~50%) of open RCs at cryogenic temperatures, avoiding nonphysiological pH values (pH >10.5) and strongly reducing agents such as dithionite in the sample (Karapetyan et al., 1997). Under these conditions the terminal iron-sulfur centers are prereduced, and the open state is maintained by fast charge recombination of the radical pair $\{P700^+ A_1^-\}$.

Fluorescence decays of both kinds of samples were recorded at 10 different wavelengths between 680 nm and 770 nm and analyzed globally. To describe the fluorescence decay kinetics for samples with all RCs closed, five lifetime components are needed: 14 ps, 35 ps, 146 ps, 401 ps, and 1.5 ns. The corresponding DAS are shown in Fig. 8 *a*. The DAS of the fastest component shows both positive amplitudes in the short-wavelength part of the spectrum (below 715 nm) and negative amplitudes toward longer wavelengths, suggesting the involvement of energy transfer processes. The other components exhibit all-positive DAS, which peak between 720 nm and 730 nm. For samples with a mixture of open and closed RCs, six lifetime components are needed for a satisfactory global fit: 18 ps, 40 ps, 184 ps, 377 ps, 1.3 ns, and 4.1 ns. The corresponding DAS are shown in Fig. 8 *b*. Also, in this case the spectrum of the fastest component changes sign and the other DAS are all positive.

To allow for a better comparison between the picosecond fluorescence kinetics and the changes in fluorescence quantum yield as revealed by fluorescence induction experiments (see Figs. 3 and 4), we also present the picosecond data of Fig. 8 as decay-associated fluorescence yield spectra in Fig. 9. Here the DAS of each component is multiplied by its respective lifetime, and the relative contribution of each decay component to the steady-state quantum yield is obtained. It is obvious from Fig. 9 *a* that in PS I with closed RCs the steady-state fluorescence is dominated by the ~401-ps component (peaking at 730 nm), whereas in the mixed open/closed sample (Fig. 9 *b*) the fluorescence yield of the 1.3-ns component with a red-shifted peak around 736 nm is slightly higher than that of the 377-ps component. Furthermore, in the mixed sample, an additional 4.1-ns component carries some 10% of the fluorescence yield at its maximum. Interestingly, this decay component has a fluorescence maximum at a wavelength of ~747 nm. An emission maximum shifted so far to the red has not been reported before for *S. elongatus*. Assuming a Stokes shift of 11 nm,

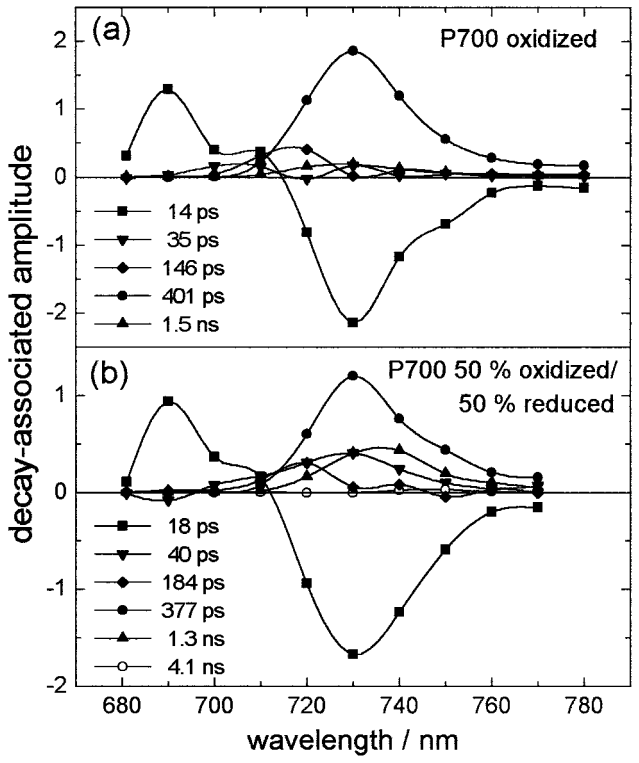

FIGURE 8 Decay-associated fluorescence amplitude spectra (DAAS) for PS I samples at 5 K with (*a*) P700 oxidized (closed PS I) and (*b*) ~50%/~50% of P700 reduced/oxidized. Note the nonconservative transfer spectrum associated with the 14-ps and 18-ps lifetimes.

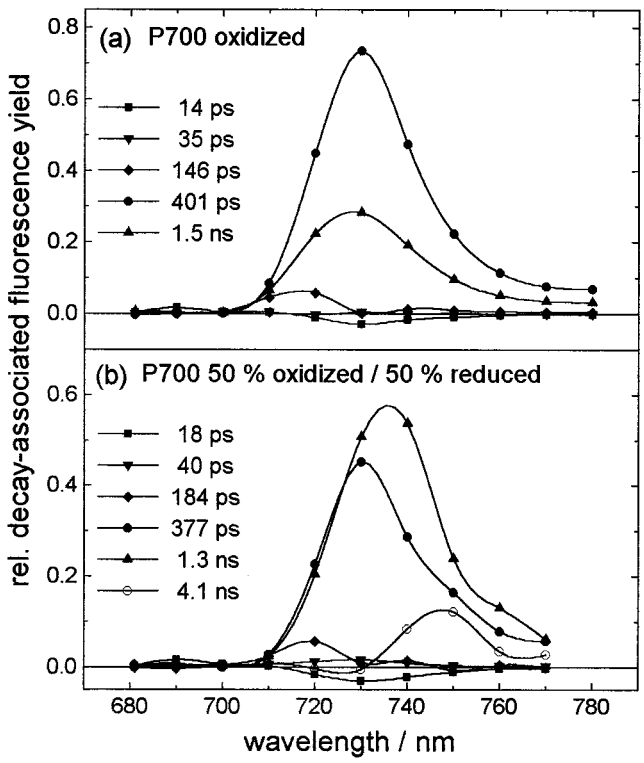

FIGURE 9 Decay-associated fluorescence quantum yield spectra (DAQYS) for PS I complexes at 5 K with (*a*) P700 oxidized (closed PS I) and (*b*) ~50%/~50% of P700 reduced/oxidized. The yields of the different components are normalized to sum to the steady-state spectra.

as determined for the longest absorbing pigments ($\lambda_A = 720$ nm) described so far for *S. elongatus* (Pålsson et al., 1996), an absorption maximum of 736 nm results for this pigment. Indeed, the 5 K absorption spectrum of the particles still has a noticeable intensity in that extremely red region (see Fig. 1).

DISCUSSION

Different quenching efficiencies of P700 and $P700^+$ at room temperature

At room temperature, both fluorescence induction (Fig. 2) and steady-state fluorescence spectra (Fig. 5) indicate that the photooxidation of P700 leads to a decrease in the quenching efficiency of the PS I primary donor. Time-resolved fluorescence experiments reported so far were not able to resolve this difference at RT (Holzwarth et al., 1993; Turconi et al., 1993; Dorra et al., 1998). Based on these kinetic data, the fluorescence quenching properties for both open and closed RC states in PS I were considered to be equal or nearly equal in the past (for a discussion see, e.g., Sétif, 1992; Brettel, 1997). Here, for the first time, we present picosecond time-resolved fluorescence data that reveal a detectable difference in the lifetime of the excited-state decay for open and closed RC states. The increase in lifetime of ~10% upon photooxidation of P700 can fully explain the observed increase in fluorescence yield upon trap closure as detected by fluorescence induction.

The effects resolved here emphasize that it actually matters whether a sample contains the oxidized or the reduced form of P700 (or both), as there are in fact differences in their quenching efficiencies. It should be noted that the exact extent of these differences depends on the size and pigment composition of the antenna, especially the content of red pigments (unpublished data). This might be an explanation for the contradictory results reported in the past (Ikegami, 1976; Telfer et al., 1978; Trissl, 1997). Furthermore, one has to be aware that application of the so-called antenna subtraction method (as described, e.g., by White et al. (1996) and Hastings et al. (1994b)) can lead to erroneous conclusions.

The excitation energy quencher in a closed RC, the oxidized primary donor $P700^+$, exhibits a broad, flat absorption that extends into the far red beyond 800 nm (Ke, 1972; Pålsson et al., 1998), which is similar to the absorption of Chl^+ in organic solvents (Davis et al., 1979; Chauvet et al., 1981). This broad absorption provides spectral overlap with the emission bands of all the core-antenna pigments, so that $P700^+$ can effectively act as an excitation energy acceptor, although the absorbance amounts to only ~1/10 of that of P700 at its absorption maximum. On this basis, the Förster overlap integral between Chl and a chlorophyll cation (Chl^+) can be estimated. With the Chl spectra of Shipman and Housman (1979) and a constant absorbance of ~7500 M^{-1} cm^{-1} for Chl^+ (Chauvet et al., 1981), one finds that the spectral overlap between Chl and Chl^+ is ~1/3 of the overlap between two isoenergetic chlorophylls, assuming a Stokes shift of 130 cm^{-1}.

With respect to the quenching mechanism, $P700^+$ provides an effective way to remove the excitation from the antenna. Its broad absorption can allow for a fast radiationless decay of higher excited states to the lowest excited state of $(P700^+)$*. This irreversibly removes the excited-state energy from the core antenna, because the energy barrier for reverse energy transfer is larger than $7k_BT$, even at RT (k_B is Boltzmann's constant, T is the absolute temperature). Thus the internal conversion from higher excited states of $(P700^+)$* to its lowest excited singlet state constitutes the quenching mechanism by $P700^+$. For general photophysical reasons, this higher excited-state decay is expected to be even faster than the consecutive decay to the ground state, i.e., on the order of ~100 fs. This fast quenching rate for the closed system has to be compared with quenching by charge separation in open PS I. No direct measurements of intrinsic charge separation rates are available for PS I. Proposed values in the range of 0.1–6 ps are based on simulations (Holzwarth et al., 1998; Gobets et al., 1998a; Jennings et al., 1997; White et al., 1996), double difference absorption transients due to A_0^- formation (Kumazaki et al., 1994), or experimentally determined values for bacterial RCs (for a review see, e.g., Woodbury and Allen, 1995).

To explain the surprisingly small difference between the fluorescence quenching efficiency of P700 and $P700^+$ at RT, various possibilities might be considered (see also Trissl, 1997): 1) The rate-limiting step is the energy transfer to the trap (Valkunas et al., 1995); both intrinsic charge separation and internal conversion occur much faster than the energy transfer to and from $P700/P700^+$. 2) The rate-limiting step is the intrinsic decay process (trap-limited); in this case (nearly) identical rate constants for charge separation from P700* and internal conversion of higher excited states of $(P700^+)$* are required. 3) In open PS I charge separation from P700* is much slower than the energy transfer to P700 (i.e., trap-limited), whereas in the closed state the intrinsic decay is much faster than energy transfer to $P700^+$ (i.e., transfer-limited). With this transfer being slowed down because of reduced spectral overlap, both effects coincidentally cancel out, and under both conditions almost identical kinetics are observed.

In the following section we will explore some characteristic features for the various kinetic regimes.

Criteria for experimental identification of a transfer limitation versus a trap limitation

Although different kinetic models for the excited-state dynamics in PS I are discussed controversially in the literature (Owens et al., 1987; Holzwarth et al., 1993; Valkunas et al., 1995; Croce et al., 1996; Jennings et al., 1997; Dorra et al.,

1998; Gobets et al., 1998a), they are nevertheless all based on rather similar experimental kinetic data. This could be due, at least in part, to the lack of unequivocal criteria needed to experimentally distinguish between the different limiting kinetics. For clarification it seems useful to utilize the concept of "transfer equilibrium" as introduced by Laible et al. (1994). Transfer equilibrium means that after the completion of all processes associated with transfer spectra, the only remaining decay process is characterized by a single-lifetime component with an all-positive spectrum, which actually reflects the mean excited-state decay from a (transfer-) equilibrated state. It is this lifetime that has been called the "mean excitation lifetime" within the framework of a transfer-limited model (Owens et al., 1987) or the "apparent charge separation time" within a trap-limited model (Holzwarth et al., 1993). The nature of the process(es) (i.e., trapping or transfer) associated with this lifetime identifies the overall antenna decay kinetics as trap limited or transfer limited or as somewhere in between. In either rate-limiting situation, moderate changes (e.g., by a factor of 2) in any of the processes except the rate-limiting one should have no considerable influence (e.g., $<$10%) on the mean lifetime observed. For a more quantitative treatment of the various kinetic models see Somsen et al. (1996).

To further explore possible characteristics of the various kinetic regimes, we consider a hypothetical antenna system that consists of just two pigment pools (see Scheme 1).

Transfer of the excitation energy from pool 1 to pool 2 takes place with a rate constant of k_{12} and vice versa with k_{21}. The ratio of the rate constants for forward and back transfers was fixed according to the detailed balance condition (Laible et al., 1998): $k_{12}/k_{21} = 80/10 \cdot \exp(-\Delta E/k_B T) = 6$ at RT (where k_B is Boltzmann's constant, T is the absolute temperature, and ΔE is the difference in transition energies for Chls in pools 1 and 2). For the following considerations we set (somewhat arbitrarily) $k_{12} = (30\ \text{ps})^{-1}$ and, consequently, $k_{21} = (180\ \text{ps})^{-1}$ and vary the rates of energy transfer out of the antenna pools into the RC (i.e., the rate constants k_{11} and k_{22}, respectively). Three different situations were considered: Fig. 10 *a*: the two antenna pools transfer excitation to the RC with equal rate constants, $k_{11} = k_{22} = (40\ \text{ps})^{-1}$; Fig. 10 *b*: transfer out of the blue pool 1 is faster by a factor of 2, $k_{11} = (20\ \text{ps})^{-1}$, $k_{22} = (40\ \text{ps})^{-1}$; and Fig. 10 *c*: the red pool 2 transfers faster by a factor of 2, $k_{11} = (40\ \text{ps})^{-1}$, $k_{22} = (20\ \text{ps})^{-1}$. For the sake of simplicity, the energy transfer from the RC back into the antenna has been neglected.

For this simplified scheme, which is merely meant to acquire some qualitative insight into nonconservative transfer spectra, two lifetimes are obtained that describe the population changes of the two antenna pools. The slower kinetic component (time constant in the range of 23–40 ps) reflects the overall decay of the excited state, while the faster one (time constant in the range of 11–16 ps) involves energy transfer between the pools. Fig. 10 shows the simulated DAS with transfer character after stoichiometric ex-

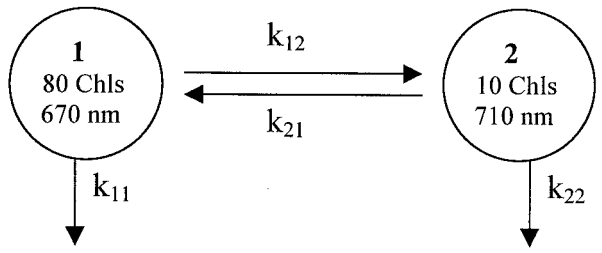

SCHEME 1 Hypothetical core-antenna system consisting of two different pools: a blue pool 1 with 80 Chls absorbing at 670 nm and a red pool 2 with 10 Chls absorbing at 710 nm. Excitation energy is transferred between the two antenna pools with rate constants k_{12} and k_{21}, which are linked to each other by the detailed-balance condition $k_{12}/k_{21} = 6$ (see text for details). Rate constants k_{11} and k_{22} describe the transfer of the energy out of the antennae into the RC.

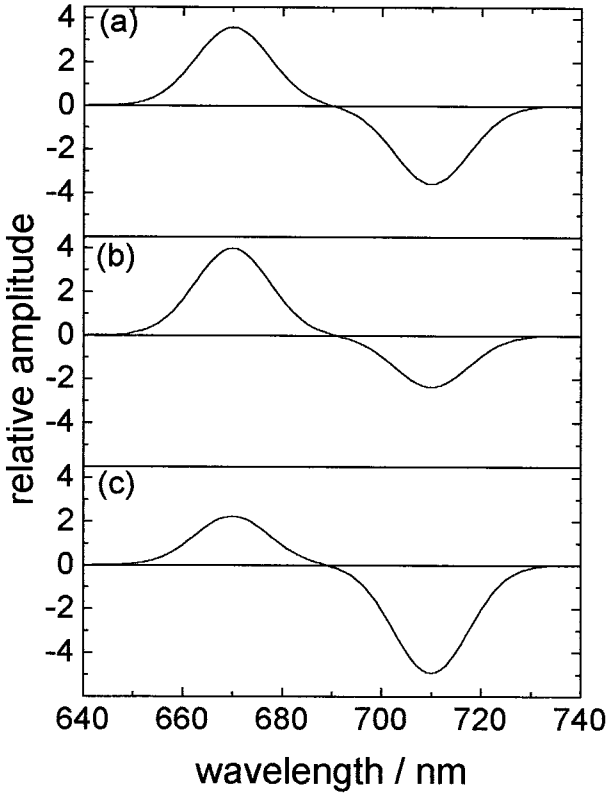

FIGURE 10 Calculated decay-associated spectra (DAS) for the hypothetical antenna system depicted in Scheme 1 (a blue pool *1* with 80 Chls absorbing at 670 nm and a red pool *2* with 10 Chls absorbing at 710 nm; excitation energy is transferred between the two antenna pools and out of the antennae into the RC; see text for details). Three different situations were considered: (*a*) both antenna pools transfer excitation to the RC with equal rate constants; (*b*) transfer out of the blue pool *1* into the RC is faster by a factor of 2; and (*c*) the red pool *2* transfers to the RC faster by a factor of 2. Note the deviations in *b* and *c* from a conservative transfer spectrum, as observed in case *a*.

citation. To allow for a better comparison with the measured DAS, the simulated amplitudes are presented as Gaussian-shaped bands, with the area enclosed by these bands being proportional to the simulated amplitudes.

It turns out that the DAS with transfer character will exhibit a conservative amplitude ratio, as long as the two quenching rates are identical, irrespective of their value relative to the transfer rates between the two pools (Fig. 10 *a*). Concomitantly, the emission DAS (not shown) reflects a Boltzmann equilibrated excitation distribution (A_1/A_2 = 1/6), as long as the sum of the transfer rate constants k_{12} and k_{21} exceeds the rate constants for the decay processes, k_{11} and k_{22}. If the blue pool 1 is quenched faster than the red pool 2 (Fig. 10 *b*), the transfer DAS becomes nonconservative in such a way as to exhibit a positive amplitude for the blue pool that is larger than the negative amplitude for the red pool. For the emission DAS (not shown), the amplitude ratio deviates significantly from Boltzmann equilibrium (A_1/A_2 = 1/10). If, on the other hand, the red pool is quenched faster than the blue pool (Fig. 10 *c*), the transfer DAS becomes nonconservative in the opposite way: The negative amplitude for the red pool is larger than the positive amplitude for the blue pool. The emission DAS (not shown) in this case exhibits an amplitude ratio of A_1/A_2 = 1/2.7.

Both nonconservative transfer spectra and non-Boltzmann-equilibrated emission spectra are experimentally accessible parameters. In the light of nonconservative transfer DAS experimentally observed in the PS I core-antenna-RC complex, the results obtained for the hypothetical two-pool-antenna model suggest that the red pigments of the core antenna are quenched faster than the (blue) bulk of the pigments and that the excited-state decay proceeds from a not completely thermally equilibrated state.

Three kinetic regimes can be distinguished, depending on the equilibrium that is established in the core-antenna-RC-complex: trap limited, transfer-to-the-trap limited, and transfer limited. Trap limitation means complete Boltzmann equilibration within the antenna as well as between antenna and RC. Transfer-to-the-trap limitation means Boltzmann equilibration within the antenna, but not between antenna and RC. Transfer limited finally means that not even within the whole core-antenna complex Boltzmann equilibrium is established before trapping occurs in the RC.

As a criterion for to what extent Boltzmann equilibrium is established in a fluorescing system, the so-called Stepanov-Kennard relation was introduced. It allows us to calculate the emission spectrum of an excited pigment from its ground-state absorption spectra, in the case where thermal equilibration is completed before emission occurs. Originally it was derived for single dye molecules (Stepanov, 1957) and has recently been adapted for the case of tightly coupled pigment clusters (Dau, 1996). Croce et al. (1996) and Jennings et al. (1997) applied the Stepanov-Kennard relation to study the extent of thermal equilibration in a PS I-200 complex from higher plants (still containing the outer light-harvesting antenna complex). (Because of the presence of the outer antenna LHCI, a direct comparison with PS I core particles should be made carefully.) They found that in the spectral region between 690 nm and 700 nm the fluorescence yield as calculated according to the Stepanov-Kennard relation is higher than the experimental observation and interpreted this as an indication that in the RC (assumed to emit in the 690–700-nm range) the excitation is quenched faster than Boltzmann equilibration can be established. Thus a transfer-to-the-trap limitation was assumed. Pålsson et al. (1998) studied PS I core-antenna-RC complexes from *S. elongatus* and found that the form of the experimentally observed fluorescence spectrum depends in a sensitive manner on the precise detergent conditions in the sample. In light of the additional problem of the arbitrary choice of the wavelength at which normalization of the measured spectra with respect to the calculated one is performed, these authors questioned the applicability of the Stepanov-Kennard relation as a useful test for equilibrium establishment. The emission spectrum presented by Pålsson et al. (1998) shows quite good agreement between calculated and measured fluorescence (after normalization at 721 nm) for almost all wavelengths, except for the short-wavelength region, where the measured values exceed the calculated ones. The better quenching of some of the red pigments with respect to the blue bulk Chls, as revealed above from the nonconservative transfer spectra, could indicate a lack of fluorescence in the red instead of an excess fluorescence in the blue range, as compared to Boltzmann equilibrium. In this alternative view, an equilibrium perturbation (Jennings et al., 1997) would concern not just the RC region but the whole red part of the emission spectrum.

The observed nonconservative transfer spectra and non-Stepanov steady-state emission spectra lead to the conclusion that Boltzmann equilibrium is not established within the core antenna. Consequently, both trap-limited and transfer-to-the-trap-limited models for the excited-state kinetics in the PS I core-antenna-RC complex seem to be inadequate. More information on the localization of the red pigments and the functioning of energy transfer can be obtained from low-temperature fluorescence kinetics, which we will consider in the next section.

Low-temperature fluorescence

The effect of increasing fluorescence yield of PS I with decreasing temperature has been attributed to the presence of red pigments, i.e., those that absorb at wavelengths longer than P700 (Satoh and Butler, 1978; Wittmershaus et al., 1992). With decreasing temperature, most of the energy transfer pathways are frozen out because of line narrowing and the reduced thermal energy available. Efficient uphill energy transfer becomes impossible, and the excitation is trapped on the energetically lowest-lying pigments. From

there it decays with a nanosecond fluorescence lifetime, close to that of isolated antenna complexes (e.g., Ide et al., 1987). This explanation, however, is only applicable in the absence of oxidized P700, i.e., for completely open PS I (Fig. 4, *triangles*). It is not stated explicitly whether this condition was established in earlier studies (see above). If, in contrast, $P700^+$ is present in the sample (Fig. 4, *squares*), its broad absorption band in the red and near infrared is able to effectively accept excitation, even from the energetically lowest-lying pigments, and subsequently quench it by internal conversion, as reflected by the weaker increase in fluorescence with decreasing temperature in this case.

In the time-resolved measurements, this difference is reflected by a 400-ps component dominating the decay kinetics in closed PS I, as compared to the nanosecond decay components prevailing in samples with open PS I (cf. Figs. 8 and 9). Taking into account that the observed 400-ps lifetime originates from two competing processes (the intrinsic nanosecond fluorescence decay as observed in open centers and direct quenching by $P700^+$), a lifetime of ~500 ps results for the latter process. Förster theory makes it possible to estimate a distance between the redmost pigments (i.e., A720) and $P700^+$ from this lifetime. With a Förster radius of 7.3 nm, as found in our simulations (see below), and the approximately threefold reduced spectral overlap with $P700^+$ (see above), a value of ~3.5 nm is calculated for this distance. This is not really far out at the periphery of the complex. However, it has to be kept in mind that this distance actually refers to the nearest of all A720 pigments, as it represents the limiting step in the process of energy transfer to $P700^+$.

A second line of information on the position of (some of) the A720 pigments is revealed by the fluorescence of mixed samples (50% open/50% closed) at 5 K. The fluorescence yield of such a mixed sample (Fig. 4, *circle*) is lower than the expected average value of samples with all RCs open (Fig. 4, *triangles*) and all RCs closed (Fig. 4, *squares*). This can be explained by the connectivity of the monomers within a trimer. The excitation in a monomer with reduced P700 is trapped on a red pigment (A720) localized at a position (e.g., in the trimerization domain) such that the excitation might well reach the oxidized P700 of a neighboring monomer within the trimer. This results in a seemingly larger fraction of PS I with closed RCs. This connectivity in mixed open/closed RC samples may also be reflected in an overall more complex decay kinetics, which cannot simply be described as a linear combination of the kinetics in samples with all RCs open and all RCs closed.

A third argument suggesting a localization of some of the A720 pigments in the trimerization domain stems from spectral decomposition of monomeric preparations of *S. elongatus* lacking the L-subunit involved in the trimerization of PS I. These mutants contain at least two A720 pigments less than wild-type preparations (Pålsson et al., 1998). All three arguments favor a localization of the A720 pigments at a minimum distance from P700 of ~3.5 nm, most likely in the trimerization domain.

Structural/spectral information-based modeling of the excited-state transfer and decay

We now combine the structural information on PS I (positions of 89 Chls from the file 2pps.bpd of the Brookhaven Protein Databank; Schubert et al., 1997) with information on the spectral composition (cf. Fig. 1), to simulate the experimentally found excited-state kinetics at room temperature for both open and closed PS I. Apart from the structural-spectral assignment (which pigments absorb at which wavelength), two intrinsic parameters, the Förster radius (a transfer rate scaling factor) and the intrinsic charge separation rate constant, can be varied (see Materials and Methods).

As a starting point, several random assignments of the various spectral forms to the known spatial positions were tested. Generally, in addition to a single all-positive spectrum associated with the longest resulting lifetime, only a few transfer spectra with noticeable amplitudes are found. The transfer spectrum with the longest lifetime reflects the redistribution of excited-state energy from the blue antenna part into the red antenna part. To simulate the experimentally observed lifetime of this transfer component, the Förster radius has to be adjusted to ~7.3 nm and was fixed at this value for further simulations. The obtained overall decay lifetimes varied between 50 ps and 120 ps, even for an intrinsic charge separation rate constant as fast as $(0.5\ \text{ps})^{-1}$. As a rule, the decay occurs too slowly for random arrangements.

As a next attempt, all red pigments (A708 and A720) are placed in the periphery of the complex. Again, unreasonably long overall fluorescence decay lifetimes (>100 ps) are obtained. This cannot be changed by accelerating the intrinsic charge separation rate, as this in turn leads to a diminished transient population of P700, which will not accelerate the observed decay kinetics (For the extreme case of very fast quenching by $P700^+$, the apparent excitation decay lifetime becomes virtually independent of the exact intrinsic quenching rate). Reasonable fluorescence decay lifetimes (~40 ps) and transfer lifetimes (~10 ps) can be obtained only by increasing the transient population of P700*. To accomplish this, it is necessary to place some red pigments in the RC vicinity (see also Jia et al., 1992; Laible et al., 1994; Trinkunas and Holzwarth, 1996, 1997).

On the basis of the independent lines of evidence mentioned above, it appears reasonable to leave the A720 pigments in the trimerization domain and to identify the four A708 pigments with one of the two linker chlorophylls and its immediate neighbors located between the trimerization domain and RC (see Fig. 11, *top*). (It should be noted that not necessarily all of the four A708 pigments have to be located on the side toward the trimerization domain. Acceptable agreement between simulation and experiment can

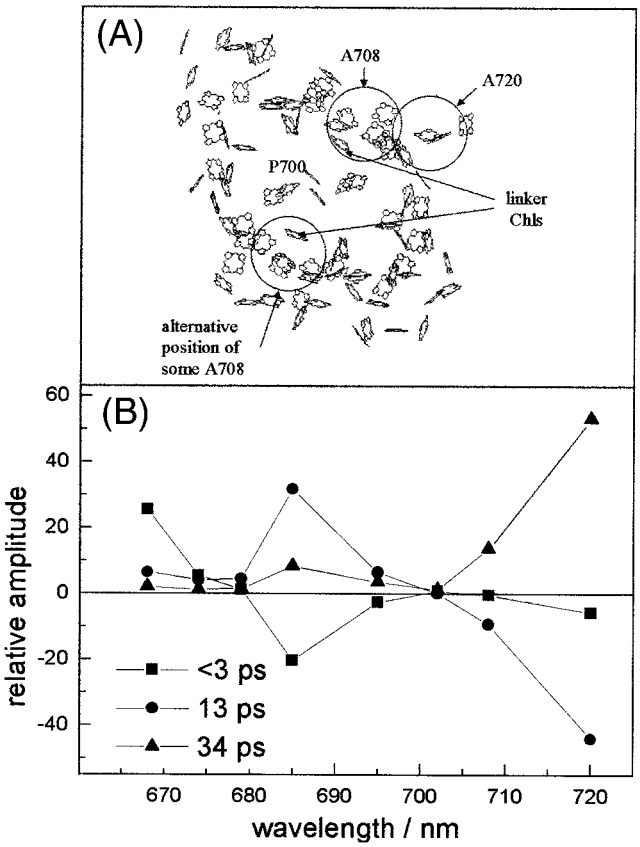

FIGURE 11 Structural/spectral information-based modeling of the energy transfer and trapping in the PS I core-antenna-RC complex from *Synechococcus el.* (*A*) Assumed arrangement of the long-wavelength antenna pigments (4xA708 and 4xA720); the possible spatial positions are indicated by the circles. The structural model of the arrangement of 89 chlorophylls is taken from the "2pps.bpd" file of the Brookhaven Protein Databank (Schubert et al.; 1997). (*B*) Calculated decay-associated "absorption" stick spectra for PS I complexes with P700 reduced (open PS I). The fast transfer spectrum (sum of all lifetime components <3 ps, ■) is beyond the time resolution of our apparatus. The slow transfer spectrum (13 ps, ●) resembles the spectrum, which has been resolved in our fluorescence decay measurements. The all-positive spectrum (34 ps, ▲) reflects the overall excited state decay from a nonequilibrated core-antenna-RC-complex.

also be obtained with a more symmetrical arrangement: up to two A708 (neighbors of the linker Chl in the arrangement depicted in Fig. 11 *A*) can be reassigned to the other linker Chl and one of its direct neighbors.) The RC chlorophylls were assumed to absorb at 695 nm to provide a spectral/spatial bridge from the A708 pigments to P700. This allocation of the A708 pigments is supported by the following experimental findings. PS I preparations from spinach, depleted of most of the core antenna chlorophylls down to 11 Chl/P700 as described by Kumazaki et al. (1994), still display some red absorption beyond P700. This speaks in favor of some A708 pigments in the vicinity of the RC. On the other hand, all of the features in the P700/P700$^+$ absorption bleach spectrum at 5 K, explained as being due to electrochromic band shifts of nearby Chls, are found on the short-wavelength side of P700 (Pålsson et al., 1998). Thus we hesitate to allocate A708 directly to the RC, but rather prefer to place it in its vicinity. The extraordinarily broad absorption of P700 (as seen from the P700/P700$^+$ difference spectrum; e.g., Pålsson et al., 1998) should nonetheless allow an efficient quenching from this A708 position. If this effect could be accounted for in the simulation, it probably would allow for pigments in the RC with an absorption maximum at ~690 nm, as found, e.g., for A_0 (Mathis et al., 1988; Hastings et al., 1994b; Kumazaki et al., 1994).

The proposed arrangement of the A708 pigments next to the RC as providers of excitation energy to P700 and of the A720 pigments in the connection domain of the trimers is shown in Fig. 11 *A*. It allows us to find a set of parameters that leads to reasonable agreement between the measured fluorescence behavior and the simulated spectra and lifetimes. For a Förster radius of 7.3 nm (for isoenergetic pigments) and the intrinsic charge separation rate constant adjusted to $(0.5\ \text{ps})^{-1}$, a transfer lifetime of 13 ps and an overall excited state decay lifetime of 34 ps were obtained. Their associated spectra resemble the measured behavior of the PSI complex (see Fig. 11 *B*). All other lifetimes are <3 ps and reflect energy transfer processes. The nonconservative character of the 13 ps transfer spectrum is not as clearly expressed as in our experimental findings (Fig. 6). This might be due partly to the presence of additional transfer components with shorter lifetimes in the simulation, which are not resolved in the picosecond experiment but have been reported in connection with recent femtosecond experiments (on *S. elongatus*: Gobets et al., 1998a; on *Synechocystis*: Savikhin et al., 1999). The steady-state emission, calculated as sum of the yields (amplitude times lifetime) over all components, shows a clear deviation from that expected according to the Stepanov-Kennard relation (not shown), in the sense that for all wavelengths greater than or equal to 695 nm, the simulated population is less than that in thermal equilibrium. Thus the simulation supports once again the nonequilibrated character of the excited-state decay as assumed in the previous section on the basis of the experimental spectra.

Preliminary modeling results by Gobets et al. (1998a,b) indicated a similar value for the intrinsic charge separation rate constant of $(0.62\ \text{ps})^{-1}$, although the overall decay time calculated there was 50 ps. Furthermore, their simulations on the excited-state dynamics in monomeric PS I core particles of *Synechocystis* indicated that the linker Chls cannot absorb at 708 nm, which would be in clear contrast to the results presented here, if the two different species/preparations were to be comparable.

The simulation described here nicely demonstrates the crucial influence of the number of the red pigments on the excitation decay time. Subsequently setting the absorption maxima of all of the red (A708 and A720) pigments to 685

nm leads to a reduction of both transfer and overall decay times down to 8 ps and 16 ps, respectively.

More importantly, the same set of parameters found to reproduce the excitation decay kinetics for open PS I, namely spectral/spatial arrangement and Förster radius, allows for a satisfactory description of the excitation decay kinetics of closed PS I as well. With an approximately threefold reduced spectral overlap between antenna pigments and $P700^+$ as compared to P700 (see above), with a rate constant of $(0.1\ ps)^{-1}$ for the internal conversion of higher excited states of $(P700^+)$*, and with an absorption maximum of the one Chl of P700 not carrying the positive charge (Käss, 1995) at ~690 nm, a transfer lifetime of 15 ps and an overall excitation decay lifetime of ~37 ps result. This demonstrates that the apparently (nearly) identical fluorescence quenching properties of reduced and oxidized P700 turn out to originate from the mutual compensation of effects of different sign due to the following underlying mechanisms. The energy transfer to the trap is slowed down in comparison to open PS I, because of reduced spectral overlap with both the oxidized and the nonoxidized P700 Chl. On the other hand, the intrinsic excitation decay proceeds on a faster time scale. Thus, for closed PS I, it seems in fact to be justified to speak of transfer-to-the-trap-limited excitation decay kinetics.

For open PS I, however, the situation is different. This can be elegantly shown by means of our structural/spectral information-based simulation, which allows us to test the influence of variations of the intrinsic parameters on the observed fluorescence behavior. Table 1 shows the change in the overall excited-state decay lifetime as the parameters governing the three different limiting regimes are varied separately by a factor of 2 (both up and down), while the other two parameters are kept constant. For the transfer-to-the-trap-limited case, all transfer rate constants into and out of the RC, along with those to and from the linking Chls, were modified. It turns out that any of the involved processes have considerable influence on the observed lifetimes, with prevailing influence by the energy transfer to the trap. With respect to the linker Chls, a functional role for the transfer of excitation energy from the antenna to the RC has been suggested (Schubert et al., 1997). The removal of the linker Chls results in a overall decay lifetime of 52 ps instead of 34 ps, thus being comparable in effect to a twofold slowing down of all transfer rates (cf. Table 1). Nonetheless, Table 1 demonstrates that the excited-state decay kinetics is neither purely trap limited nor purely transfer (to the trap) limited, but seem to be rather balanced, which appears reasonable in terms of efficiency. Thus neither of the limiting cases is realized, at least in *S. elongatus.*

TABLE 1 Dependence of the excited-state decay lifetime on the time constants for energy transfer, energy transfer to the trap, and energy trapping

Process	Slowed down twice	Speeded up twice
Transfer to the trap (i.e., to all RC Chls and the linker Chls)	74 ps	20 ps
Transfer (all transfer steps)	57 ps	22 ps
Trapping (intrinsic charge separation)	44 ps	29 ps

The numbers have to be compared with the optimal value of 34 ps. Note that all three classes of processes have considerable influence; thus the overall excited-state decay time seems to be rather balanced with the prevailing influence of the energy transfer to the trap.

CONCLUSIONS

For the first time, the excitation quenching efficiency of the PS I core-antenna-RC complex could be established to be different for open and closed PS I, by both fluorescence induction and picosecond-time-resolved fluorescence experiments, as well as by quasi-steady-state spectroscopy. The difference of $(12 \pm 5)\%$ in fluorescence yield between the open and closed RC states is due to a ~3-ps difference in the overall excitation decay lifetime. Thus the excited state is quenched slightly worse in closed PS I than in open PS I at RT.

Time-resolved fluorescence in the picosecond range could resolve nonconservative transfer spectra both at RT and at 5 K, which indicates that trapping does not occur from a completely thermally equilibrated core-antenna-RC complex. As a consequence, trap limitation for the excited-state kinetics can be excluded.

From the lifetime of the excited state at 5 K in closed PS I, an A720-P700 distance of ~3.5 nm is derived. The observed intermonomer exchange of excitation energy supports a localization of some A720 pigments in the connecting domain of the trimeric unit. Simulation of the excitation energy transfer and decay based on all available structural/spectral information strongly hints at the requirements to place some A708 pigments between the RC domain and the peripheral red pigments (A720) to increase the transient population of P700*. Based on this arrangement of the red pigments, an intrinsic charge separation rate constant of $(0.5\ ps)^{-1}$ and a Förster radius of 7.3 nm are obtained as optimal parameters. Moreover, the simulation indicates a nonequilibrium distribution of the excitation energy and reveals a determining influence of the red pigments. For open PS I the observable excited-state decay is characterized by balanced kinetics rather than limiting cases. The kinetics in closed PS I can be described by the same value for the Förster radius combined with a fast quenching via internal conversion.

We thank Prof. Dr. H. T. Witt and Dr. P. Fromme for providing the PS I complexes, which were skillfully prepared by D. DiFiore and C. Lüneberg. We are very grateful to Marianne Çetin for excellent technical assistance.

This work was supported by the Deutsche Forschungsgemeinschaft (Sfb 498 and Sfb 312).

REFERENCES

Beechem, J. M., E. Gratton, M. Ameloot, J. R. Knutson, and L. Brand. 1991. The global analysis of fluorescence intensity and anisotropy decay data: second generation theory and programs. *In* Topics in Fluorescence Spectroscopy, Vol. 2: Principles. J. R. Lakowicz, editor. Plenum Press, New York. 241–305.

Beddard, G. S. 1998. Excitations and excitons in photosystem I. *Philos. Trans. R. Soc. Lond. A.* 356:421–448.

Borisov, A. Y. 1989. Transfer of excitation energy in photosynthesis: some thoughts. *Photosynth. Res.* 20:35–58.

Brettel, K. 1997. Electron transfer and arrangement of the redox cofactors in photosystem I. *Biochim. Biophys. Acta.* 1318:322–373.

Byrdin, M. 1999. Messungen und Modellierungen zur Dynamik angeregter Zustände in Photosystem I. Ph.D. thesis. Free University Berlin.

Byrdin, M., I. Rimke, C. Flemming, E. Schlodder, and T. A. Roelofs. 1998. Excitation energy transfer and trapping in PS I: fluorescence induction and picosecond fluorescence kinetics. *In* Photosynthesis: Mechanisms and Effects. G. Garab, editor. Kluwer Academic Publishers, Dordrecht, the Netherlands. 567–570.

Chauvet, J.-P., R. Viovy, R. Santos, and E. J. Land. 1981. One electron oxidation of photosynthetic pigments in micelles. Bacteriochlorophyll a, chlorophyll a, chlorophyll b and pheophytin a. *J. Phys. Chem.* 85: 3449–3456.

Colbow, K. 1973. Energy transfer in photosynthesis. *Biochim. Biophys. Acta.* 314:320–327.

Croce, R., G. Zucchelli, F. M. Garlaschi, R. Bassi, and R. C. Jennings. 1996. Excited state equilibration in the photosystem I-light-harvesting I complex: P700 is almost isoenergetic with its antenna. *Biochemistry.* 35:8572–8579.

Dau, H. 1996. On the relation between absorption and fluorescence emission spectra of photosystems: derivation of a Stepanov relation for pigment clusters. *Photosynth. Res.* 48:139–145.

Davis, M. S., A. Forman, and J. Fajer. 1979. Ligated chlorophyll cation radicals: their function in photosystem II of plant photosynthesis. *Proc. Natl. Acad. Sci. USA.* 76:4170–4174.

DiMagno, L., C.-K. Chan, Y. Jia, M. J. Lang, J. R. Newman, L. Mets, G. R. Fleming, and R. Haselkorn. 1995. Energy transfer and trapping in photosystem I reaction centers from cyanobacteria. *Proc. Natl. Acad. Sci. USA.* 92:2715–2719.

Dorra, D. 1998. Funktionelle Organisation des Photosystem I: Pikosekundenaufgelöste Fluoreszenzuntersuchungen. Ph.D. thesis. Düsseldorf/ Mülheim a.d. Ruhr, Germany.

Dorra, D., P. Fromme, N. V. Karapetyan, and A. R. Holzwarth. 1998. Fluorescence kinetics of photosystem I: multiple fluorescence components. *In* Photosynthesis: Mechanisms and Effects. G. Garab, editor. Kluwer Academic Publishers, Dordrecht, the Netherlands. 587–590.

Flemming, C. 1996. Charakterisierung der Antennensysteme von monomeren und trimeren Photosystem I Komplexen. Diploma work. Technische Universität, Berlin.

Fromme, P., and H. T. Witt. 1998. Improved isolation and crystallization of photosystem I for structural analysis. *Biochim. Biophys. Acta.* 1365: 175–184.

Gobets, B., J. P. Dekker, and R. van Grondelle. 1998a. Transfer-to-the-trap limited model of energy transfer in photosystem I. *In* Photosynthesis: Mechanisms and Effects. G. Garab, editor. Kluwer Academic Publishers, Dordrecht, the Netherlands. 503–508.

Gobets, B., H. van Amerongen, R. Monshouwer, J. Kruip, M. Rögner, R. van Grondelle, and J. P. Dekker. 1994. Polarized site-selected fluorescence spectroscopy of isolated photosystem I particles. *Biochim. Biophys. Acta.* 1188:75–85.

Gobets, B., I. H. M. van Stokkum, F. van Mourik, M. Rögner, J. Kruip, J. P. Dekker, and R. van Grondelle. 1998b. Time resolved fluorescence measurements of photosystem I from *Synechocystis* PCC 6803. *In* Photosynthesis: Mechanisms and Effects. G. Garab, editor. Kluwer Academic Publishers, Dordrecht, the Netherlands. 571–574.

Golbeck, J. H. 1994. Photosystem I in cyanobacteria. *In* The Molecular Biology of Cyanobacteria. D. A. Bryant, editor. Kluwer Academic Publishers, Dordrecht, the Netherlands. 319–360.

Hastings, G., F. A. M. Kleinherenbrink, S. Lin, and R. E. Blankenship. 1994a. Time-resolved fluorescence and absorption spectroscopy of photosystem I. *Biochemistry.* 33:3185–3192.

Hastings, G., F. A. M. Kleinherenbrink, S. Lin, T. J. McHugh, and R. E. Blankenship. 1994b. Observation of the reduction and reoxidation of the primary electron acceptor in photosystem I. *Biochemistry*. 33: 3193–3200.

Hastings, G., L. J. Reed, S. Lin, and R. E. Blankenship. 1995. Excited state dynamics in photosystem I: effects of detergent and excitation wavelength. *Biophys. J.* 69:2044–2055.

Holzwarth, A. R., D. Dorra, M. G. Müller, and N. V. Karapetyan. 1998. Structure-function relationships and excitation dynamics in photosystem I. *In* Photosynthesis: Mechanisms and Effects. G. Garab, editor. Kluwer Academic Publishers, Dordrecht, the Netherlands. 497–502.

Holzwarth, A. R., G. Schatz, H. Brock, and E. Bittersmann. 1993. Energy transfer and charge separation kinetics in photosystem I. Part I: picosecond transient absorption and fluorescence study of cyanobacterial photosystem I particles. *Biophys. J.* 64:1813–1826.

Ide, J. P., D. R. Klug, W. Kühlbrandt, L. B. Giorgi, and G. Porter. 1987. The state of detergent solubilised light-harvesting chlorophyll-a/b protein complex as monitored by picosecond time-resolved fluorescence and circular dichroism. *Biochim. Biophys. Acta.* 893:349–364.

Ikegami, I. 1976. Fluorescence changes related to the primary photochemical reaction in the P700 enriched particles isolated from spinach chloroplasts. *Biochim. Biophys. Acta.* 449:245–258.

Jennings, R. C., G. Zucchelli, R. Croce, L. Valkunas, L. Finzi, and F. M. Garlaschi. 1997. Model studies on the excited state equilibrium perturbation due to reaction centre trapping in photosystem I. *Photosynth. Res.* 52:245–253.

Jia, Y., J. M. Jean, M. M. Werst, C.-K. Chan, and G. R. Fleming. 1992. Simulation of the temperature dependence of energy transfer in the PS I core antenna. *Biophys. J.* 63:259–273.

Kakitani, T., A. Kimura, and H. Sumi. 1999. Theory of excitation transfer in the intermediate coupling case. *J. Phys. Chem.* 103:3720–3726.

Karapetyan, N. V., D. Dorra, G. Schweitzer, I. N. Bezsmertnaya, and A. R. Holzwarth. 1997. Fluorescence spectroscopy of the longwave chlorophylls in trimeric and monomeric photosystem I core complexes from the cyanobacterium *Spirulina platensis. Biochemistry.* 36:13830–13837.

Käss, H. 1995. Die Struktur des primären Donators in Photosystem I. Ph.D. thesis. Technische Universität, Berlin.

Ke, B. 1972. The rise time of photoreduction, difference spectrum and oxidation reduction potential of P430. *Arch. Biochem. Biophys.* 152: 70–77.

Klukas, O., W.-D. Schubert, P. Jordan, N. Krauss, P. Fromme, H. T. Witt, and W. Saenger. 1999. Localization of two phylloquinones Q_K and Q_K' in an improved electron density map of photosystem I at 4 Å resolution. *J. Biol. Chem.* 274:7361–7367.

Krause, G. H., and E. Weis. 1991. Chlorophyll fluorescence and photosynthesis: the basics. *Annu. Rev. Plant Physiol. Plant Mol. Biol.* 42:313–349.

Kumazaki, S., H. Kandori, H. Petek, K. Yoshihara, and I. Ikegami. 1994. Primary photochemical processes in P700-enriched photosystem I particles: trap-limited excitation decay and primary charge separation. *J. Phys. Chem.* 98:10335–10342.

Laible, P. D. 1995. The first 100 picoseconds of photosynthesis: excited state energy transfer and trapping in photosystem I. Ph.D. thesis. Cornell University.

Laible, P. D., R. S. Knox, and T. G. Owens. 1998. Detailed balance in Förster-Dexter excitation transfer and its application to photosynthesis. *J. Phys. Chem.* 102:1641–1648.

Laible, P. D., W. Zipfel, and T. G. Owens. 1994. Excited state dynamics in chlorophyll-based antennae: the role of transfer equilibrium. *Biophys. J.* 66:844–860.

Mathis, P., I. Ikegami, and P. Sétif. 1988. Nanosecond flash studies of the absorption spectrum of the photosystem I primary acceptor A_0. *Photosynth. Res.* 16:203–210.

Owens, T. G., S. P. Webb, L. Mets, R. S. Alberte, and G. R. Fleming. 1987. Antenna size dependence of fluorescence decay in the core antenna of photosystem I: estimates of charge separation and energy transfer rates. *Proc. Natl. Acad. Sci. USA.* 84:1532–1536.

Pålsson, L.-O., J. P. Dekker, E. Schlodder, R. Monshouwer, and R. van Grondelle. 1996. Polarized site-selective fluorescence spectroscopy of the long wavelength emitting chlorophylls in isolated photosystem I particles from *Synechococcus elongatus. Photosynth. Res.* 48:239–246.

Pålsson, L.-O., C. Flemming, B. Gobets, R. van Grondelle, J. P. Dekker, and E. Schlodder. 1998. Energy transfer and charge separation in photosystem I: P700 oxidation upon selective excitation of the long-wavelength antenna chlorophylls of *Synechococcus elongatus. Biophys. J.* 74:2611–2622.

Pålsson, L.-O., S. E. Tjus, B. Andersson, and T. Gillbro. 1995. Energy transfer in photosystem I. Time resolved fluorescence of the native photosystem I complex and its core complex. *Chem. Phys.* 194:291–302.

Pearlstein, R. M. 1982. Exciton migration and trapping in photosynthesis. *Photochem. Photobiol.* 35:835–844.

Satoh, K., and W. L. Butler. 1978. Low temperature spectral properties of subchloroplast fractions purified from spinach. *Plant Physiol.* 61: 373–379.

Savikhin, S., W. Xu, V. Soukolis, P. R. Chitnis, and W. S. Struve. 1999. Ultrafast primary processes in photosystem I of *Synechocystis PCC 6803. Biophys. J.* 76:3278–3288.

Schlodder, E., K. Falkenberg, M. Gergeleit, and K. Brettel. 1998. Temperature dependence of forward and reverse electron transfer from A_1^-, the reduced secondary electron acceptor in photosystem I. *Biochemistry.* 37:9466–9476.

Schubert, W.-D., O. Klukas, N. Krauss, W. Saenger, P. Fromme, and H. T. Witt. 1997. Photosystem I of *Synechococcus elongatus* at 4 Å resolution: comprehensive structure analysis. *J. Mol. Biol.* 272:741–769.

Sétif, P. 1992. Energy transfer and trapping in photosystem I. *In* The Photosystems: Structure, Function and Molecular Biology. J. Barber, editor. Elsevier Science Publishers, Amsterdam. 471–499.

Shipman, L. L., and D. L. Housman. 1979. Förster transfer rates for chlorophyll *a. Photochem. Photobiol.* 29:1163–1167.

Somsen, O. J. G., L. Valkunas, and R. van Grondelle. 1996. A perturbed two-level model for exciton trapping in small photosynthetic systems. *Biophys. J.* 70:669–683.

Stepanov, B. I. 1957. Universal relationship between absorption and luminescence spectra of complex molecules. *Dokl. Akad. Nauk SSSR.* 112: 839–841.

Telfer, A., J. Barber, P. Heathcote, and M. C. W. Evans. 1978. Variable chlorophyll *a* fluorescence from P700 enriched photosystem I particles dependent on the redox state of the reaction centre. *Biochim. Biophys. Acta.* 504:153–164.

Trinkunas, G., and A. R. Holzwarth. 1994. Kinetic modeling of exciton migration in photosynthetic systems. 2. Simulations of excitation dynamics in two-dimensional photosystem I core-antenna-RC-complexes. *Biophys. J.* 66:415–429.

Trinkunas, G., and A. R. Holzwarth. 1996. Kinetic modeling of exciton migration in photosynthetic systems. 3. Application of genetic algorithms to simulations of excitation dynamics in three-dimensional photosystem I core-antenna-RC-complexes. *Biophys. J.* 71:351–364.

Trinkunas, G., and A. R. Holzwarth. 1997. On the rate-limiting process of energy transfer in the light harvesting antenna. *J. Lumin.* 72–74: 615–617.

Trissl, H.-W. 1993. Long wavelength absorbing antenna pigments and heterogeneous absorption bands concentrate excitons and increase absorption cross section. *Photosynth. Res.* 35:247–263.

Trissl, H.-W. 1997. Determination of the quenching efficiency of the oxidized primary donor of photosystem I, $P700^+$: implications for the trapping mechanism. *Photosynth. Res.* 54:237–240.

Turconi, S., G. Schweitzer, and A. R. Holzwarth. 1993. Temperature dependence of picosecond fluorescence kinetics of a cyanobacterial photosystem I particle. *Photochem. Photobiol.* 57:113–119.

Turconi, S., N. Weber, G. Schweitzer, H. Strotmann, and A. R. Holzwarth. 1994. Energy transfer and charge separation kinetics in photosystem I. 2. Picosecond fluorescence study of various PS I particles and light-harvesting complex isolated from higher plants. *Biochim. Biophys. Acta.* 1187:324–334.

Valkunas, L., L. Liuolia, J. P. Dekker, and R. van Grondelle. 1995. Description of energy migration and trapping in photosystem I by a model with two distance scaling parameters. *Photosynth. Res.* 43: 149–154.

Van Grondelle, R. 1985. Excitation energy transfer, trapping, annihilation in photosynthetic systems. *Biochim. Biophys. Acta.* 811:147–195.

Van Grondelle, R., J. P. Dekker, T. Gillbro, and V. Sundström. 1994. Energy transfer and trapping in photosynthesis. *Biochim. Biophys. Acta.* 1187:1–65.

Webber, A. N., H. Su, S. E. Bengham, H. Kaff, L. Krabben, M. Kuhn, R. Jordan, E. Schlodder, and W. Lubitz. 1996. Site-directed mutations effecting the spectroscopic characteristics and midpoint potential of the primary donor in photosystem I. *Biochemistry.* 35:12857–12863.

Werst, M., Y. Jia, L. Mets, and G. R. Fleming. 1992. Energy transfer and trapping in the photosystem I core antenna. A temperature study. *Biophys. J.* 61:868–878.

White, N. T. H., G. S. Beddard, J. R. G. Thorne, T. M. Feehan, T. E. Keyes, and P. Heathcote. 1996. Primary charge separation and energy transfer in the photosystem I reaction center of higher plants. *J. Phys. Chem.* 100:12086–12099.

Wittmershaus, B. P., V. M. Woolf, and W. F. J. Vermaas. 1992. Temperature dependence and polarization of fluorescence from photosystem I in the cyanobacterium *Synechocystis sp.* PCC 6803. *Photosynth. Res.* 31: 75–87.

Woodbury, N. W., and J. P. Allen. 1995. The pathways, kinetics and thermodynamics of electron transfer in wild type and mutant reaction centers of purple nonsulfur bacteria. *In* Anoxygenic Photosynthetic Bacteria. R. E. Blankenship, M. T. Madigan, and C. E. Bauer, editors. Kluwer, Dordrecht, the Netherlands. 527–557.